Nanoscale Advances

ROYAL SOCIETY OF CHEMISTRY

PAPER

View Article Online
View Journal

Cite this: DOI: 10.1039/d5na00731c

Dynamic glycan network engineering of native mucin enables reversible, self-healing, and adhesive hydrogel interfaces

Yuki Nakamura,[a] Kanta Numata,[a] Momoka Hirosaki,[a] Hiroki Miyajima [ab] and Satoshi Fujita *[ab]

Mucin, a glycoprotein with a network-like structure of O-linked oligosaccharides, is a major component of the mucus layer and is essential for lubricating tissues, protecting against pathogens and chemicals, and maintaining intestinal symbiosis. Mucin-based hydrogels are promising for biomedical applications; however, conventional mucin hydrogels typically require chemical crosslinking, which involves complex procedures that cause irreversible structural changes. In this study, we developed a physically crosslinked mucin hydrogel *via* pH-dependent interactions between the diol groups of mucin oligosaccharides and boric acid (BA) without using chemical crosslinkers. This hydrogel was prepared by simply mixing porcine gastric mucin (PGM) and BA, followed by pH adjustment. It exhibited reversible gelation and tunable mechanical strength depending on PGM and BA concentrations. Increased gel strength was associated with increased crosslink density and reduced mesh size, which are attributed to dense multipoint crosslinking *via* the branched structure of mucin. The hydrogel demonstrated rapid self-healing within 1 min, strong adhesion to glass, and retention of mechanical integrity after ultraviolet (UV) irradiation, indicating compatibility with UV-based sterilization. These features highlight its potential as a reversible hydrogel for cell culture, tissue adhesives, and wound healing applications.

Received 31st July 2025
Accepted 27th December 2025

DOI: 10.1039/d5na00731c

rsc.li/nanoscale-advances

Introduction

Self-healing hydrogels composed of proteins and polymers feature networks that can recombine after damage through dynamic association–dissociation interactions, thereby exhibiting self-healing properties. Self-healing properties are driven by noncovalent interactions such as hydrogen bonding, electrostatic interactions, metal coordination, π–π stacking between aromatic rings, and host–guest interactions. Because these interactions dissociate and reform more easily than covalent bonds, they are suitable for rapid self-healing. In addition to self-healing, adhesion to biological surfaces is a crucial feature of biomedical hydrogels, particularly in wound dressings and tissue adhesives, where close contact with tissues is essential.

In this study, we focused on mucin, a glycoprotein. In humans and animals, organs exposed to the external environment, such as the eyes, nose, mouth, stomach, and intestines, are covered with mucus layers.[1] Mucin is the primary component of these layers[2] and comprises a long-chain core protein and numerous O-linked oligosaccharides. The molecular weight of mucin ranges from several kilodaltons to megadaltons, with the majority of its mass derived from oligosaccharides.[3–5] The core protein contains functional domains, such as the von Willebrand factor and cysteine-rich domains, which facilitate the formation of gel-like networks in mucin through intermolecular interactions.[3,6–11]

The mucin-based mucus layer serves multiple functions in the body, including lubricating tissues,[2] protecting against pathogens and chemicals,[12] and supporting symbiosis with intestinal microbiota.[13,14] A structural feature of mucin is its interpenetrating double network, which is composed of negatively charged polymers and positively charged proteins.[15] Studies on snail mucin have shown that this network structure imparts strong adhesive and energy-dissipating properties.[16] These unique bioadhesive and viscoelastic properties make mucin a promising material for use in bioinspired hydrogels.

Recently, mucin-based biomaterials have been developed for applications in cell culture and medicine, such as wound healing. These biomaterials include gels,[17–20] films[21] and fibers.[22,23] Several mucin-based hydrogels have been synthesized using chemical crosslinking strategies, such as introducing aldehyde and hydrazine linkers,[18] forming disulfide bonds between cysteine-rich regions and thiolated polyethylene glycol (PEG),[19] and using catechol–thiol bonds.[20] However, these chemical modifications irreversibly alter the structure of mucin, limiting its applicability as a reversible, self-healing, and

[a]*Department of Frontier Fiber Technology and Science, University of Fukui, 910-8507, Fukui, Japan. E-mail: fujitas@u-fukui.ac.jp*

[b]*Life Science Innovation Center, University of Fukui, 910-8507, Fukui, Japan*

biocompatible material, particularly under sterilized conditions.

To address these limitations, researchers have developed self-healing hydrogels composed of polymers containing mucin and phenylboronic acid. Tao *et al.* developed a hydrogel based on dynamic boronate ester bonds formed between mucin-derived diols and phenylboronic acid groups.[24] Bej *et al.* designed a mucin-inspired copolymer by introducing disulfide linkages into sulfated polyglycerol dendrimers, enabling self-healing through reversible disulfide exchange reactions using PEG-based thiol crosslinkers.[25]

We aimed to fabricate a reversible, self-healing mucin hydrogel without irreversible chemical modifications. To this end, we focused on the physical crosslinking between diols from mucin oligosaccharides and boric acid (BA). BA offers several advantages: it eliminates the need for the chemical modification of polymers, offers high biocompatibility owing to its simple and nonaromatic structure, and improves stability under sterilization conditions such as ultraviolet (UV) irradiation. The interactions between diols and BA are well established in poly(vinyl alcohol)/BA hydrogels,[26,27] in which gelation is reversible and pH-dependent.[27,28] Mucin contains backbone sugars, such as galactose and *N*-acetylgalactosamine, and terminal sugars, such as sialic acid and fucose,[29,30] which contain diol structures. We hypothesized that mucin could form reversible hydrogels with BA *via* physical crosslinking. Unlike linear PVA, mucin carries densely branched O-linked oligosaccharides that provide numerous *cis*-diol groups, enabling multivalent and heterogeneous borate–diol crosslinking as illustrated in Scheme 1. To evaluate this reversible gelation, we primarily employed rheological analyses, which sensitively capture the formation and dissociation of dynamic BA–diol crosslinks.

Given the importance of sterilization in biomedical applications, we investigated whether the hydrogel structure could be retained after UV irradiation because mucin is sensitive to heat, autoclaving, and γ-ray irradiation.[31] In this study, we constructed a weak yet multivalent network inspired by the mucus layer architecture, achieving reversible gelation, self-healing, strong adhesiveness, UV resistance, and tunable mechanical properties without chemical modification. Mucin-based hydrogels are promising functional materials for future biomedical applications.

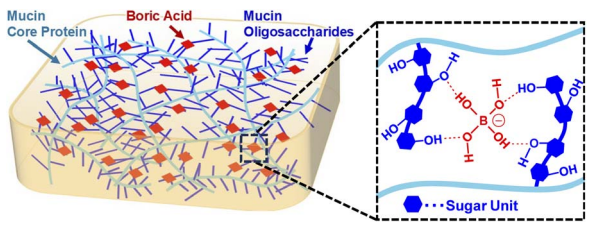

Scheme 1 Schematic illustration of the reversible crosslinking mechanism in the PGM–borate hydrogel. Mucin consists of a protein core decorated with densely packed O-linked oxligosaccharides that present multiple *cis*-diol groups. Boric acid forms dynamic borate–diol complexes with these glycans, generating reversible BO_3/BO_4-type crosslinks between mucin chains. The multivalent and heterogeneous distribution of oligosaccharides enables a three-dimensional, physically crosslinked network distinct from linear PVA–borate systems.

Experimental

Materials

Porcine gastric mucin (PGM) powder was purchased from FUJIFILM Wako Pure Chemical Corporation (Osaka, Japan). BA was purchased from KOZAKAI Pharmaceutical Co., Ltd (Tokyo, Japan). Hydrochloric acid (HCl) and sodium hydroxide (NaOH) were purchased from FUJIFILM Wako Pure Chemical Co (Osaka, Japan). Rhodamine 6G and methylene blue powders were purchased from Tokyo Chemical Industry Co., Ltd (Tokyo, Japan) and FUJIFILM Wako Pure Chemical Corporation (Osaka, Japan), respectively. Ultrapure water was prepared using a Milli-Q IQ7000 system (Merck Millipore, Burlington, MA, USA). Polyethylene bags for sterilizing PGM/BA hydrogels were purchased from SEISANNIPPONSHA Ltd (Osaka, Japan).

Preparation of the PGM/BA hydrogels

PGM and BA were dissolved separately in water by stirring at room temperature. The PGM/BA hydrogels were prepared by mixing PGM and BA solutions, and the pH was adjusted using 1 mol L^{-1} HCl or 1 mol L^{-1} NaOH as needed. The pH was measured using a pH meter (F-72; HORIBA, Ltd, Kyoto, Japan). To improve the gel uniformity, we repeatedly mixed the resulting gel using a glass stick.

Rheological measurements

Rheological measurements were performed using a compact modular rheometer (MCR302e, Anton Paar, Graz, Austria). The geometry was selected based on the sample viscosity: either a 25 mm diameter and 2° cone plate (CP25-2) or a 50 mm diameter and 1° cone plate (CP50-1). Strain sweep measurements were conducted from 0.1% to 100% strain at a frequency of 1 rad s^{-1}. Frequency sweep measurements were conducted from 10 to 0.1 rad s^{-1} at 10% strain. The sample plate temperature was maintained at 21 °C.

Self-healing test

The PGM/BA hydrogel was prepared by mixing 10% PGM with 300 mM BA, and the pH was adjusted to 8.0. Rhodamine 6G and methylene blue dyes were separately dissolved in water to form a 1% solution. To stain the hydrogel, we added 20 μL of dye solution to 1 g of hydrogel and mixed with a glass stick. The stained gels were shaped into 10 mm–diameter half-spheres and cut in half using a spatula. The cut surfaces were brought into contact and gently pressed using a spatula. After allowing the gels to stand for 1 min, they were manually pulled from both ends. These processes were recorded using a digital camera (TG-4; Olympus Corporation, Tokyo, Japan).

Adhesive test

The PGM/BA hydrogel was prepared by mixing 10% PGM with 300 mM BA, and the pH was adjusted to 8.0. The hydrogel was placed on a glass plate, and a glass beaker was placed on top of the gel. The gel was sandwiched between the glass plate and the bottom of the beaker by applying pressure for approximately 10 s. After pressing, the beaker was lifted by grasping its side to determine whether the glass plate adhered to the beaker.

UV irradiation of the PGM/BA hydrogel

The PGM/BA hydrogel was prepared by mixing 10% PGM with 300 mM BA, and the pH was adjusted to 8.0. The gels were packed in transparent polyethylene bags, flattened, and irradiated with UV light using an SX-UI500H USHIO Optical Module X (Ushio Inc., Tokyo, Japan) equipped with a high-pressure mercury lamp (HPML). The UV irradiance was maintained at 15 mW cm^{-2} using an illuminance meter (IM-213; RS Americas Inc., TX, USA).

Results and discussion

PGM and BA form a reversible hydrogel depending on pH

Mucin is an oligosaccharide-rich glycoprotein[29,30] with diol structures in some sugar chains. We hypothesized that mixing mucin with BA and adjusting the pH would induce physical crosslinking, resulting in the formation of a mucin/BA hydrogel.

A mixture of 5% PGM and 300 mM BA was prepared, and the pH was adjusted to 7.0, 7.5, 8.0, or 9.0. The rheological properties of the PGM/BA mixtures were evaluated using a rheometer (Fig. 1). At pH 7.0, the storage modulus (G') was lower than the loss modulus (G''), and the sample appeared sol-like. As the pH increased, G' gradually increased, and the appearance of PGM/BA mixture shifted from sol-like to gel-like. At 10 rad s^{-1}, G' exceeded G'' when the pH was above 7.5, indicating gel formation (Fig. 1e). This gelation was reversible and pH-dependent (Fig. 1f).

At pH 9.0, G' and G'' were slightly lower than those at pH 8.0. O-linked glycans can cleave from the core protein *via* β-elimination under basic conditions.[32,33] This decrease in rheological strength may be due to the gradual release of O-glycans from mucin at pH 9.0 or rapid cleavage caused by the use of 1 mol L^{-1} NaOH for pH adjustment, potentially compromising gel integrity. Excessively high pH and base concentration can negatively affect gel formation. However, this issue can be mitigated by adjusting the pH to a near-neutral range (*e.g.*, 7.5–8.0) using a low-concentration base (*e.g.*, 0.1 mol L^{-1} NaOH).

PVA/BA hydrogels also form *via* BA-induced crosslinking,[26,27] where pH plays a crucial role.[28] This crosslinking is attributed to the pH-dependent changes in the structure of BA: below pH 7.0, BA exists as $B(OH)_3$ (orthoboric acid), whereas above pH 7.0, it gradually converts to $B(OH)_4^-$ (tetrahydroxyborate).[34] The $B(OH)_4^-$ species can reversibly form physical crosslinks with PVA-derived diols, forming PVA/BA hydrogel.[35] The results shown in Fig. 1f indicate that PGM/BA hydrogel formation also occurred at approximately pH 7.5, which is consistent with the behavior of PVA/BA hydrogels. Therefore, we conclude that PGM forms reversible hydrogels *via* physical crosslinking with BA. This physical crosslinking is further supported by FTIR analysis (Fig. S1), in which characteristic spectral changes associated with borate–diol complexation were observed.

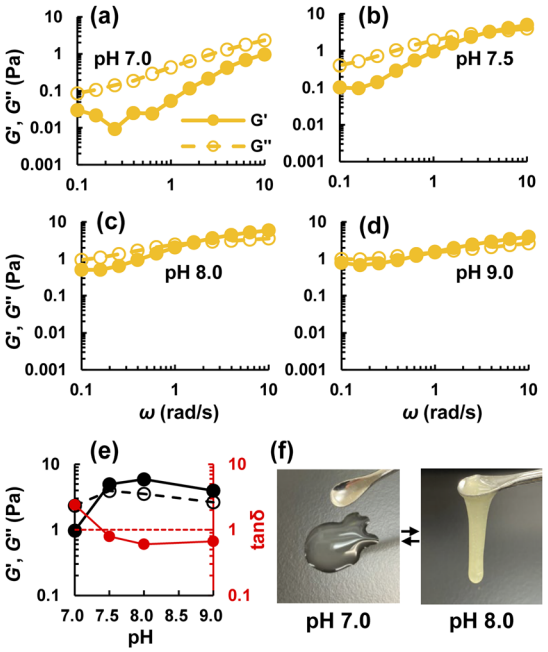

Fig. 1 Rheological characterization of the PGM/BA mixtures at different pH values. Frequency sweep measurements (10% strain) were conducted on mixtures containing 5% PGM and 300 mM BA at pH values of (a) 7.0, (b) 7.5, (c) 8.0, and (d) 9.0. Filled and open circles represent the storage modulus (G') and loss modulus (G''), respectively. (e) G', G'' and loss tangent (tanδ) values at 10 rad s^{-1} plotted as a function of pH. (f) Macroscopic appearance of the mixtures at pH 7.0 and 8.0, showing the pH-responsive sol–gel transition behavior.

PGM/BA hydrogel gel strength varies with BA concentration

In the previous section, we confirmed that PGM forms a hydrogel *via* physical crosslinking with BA and that this gelation is reversible and pH-dependent. Previous studies have shown that the gel strength of PVA/BA hydrogels varies with the concentrations of PVA and BA.[27] Similarly, we anticipated that the gel strength of the PGM/BA hydrogels would change with the PGM and BA concentrations. We evaluated the effect of BA concentration on gel strength.

PGM/BA mixtures were prepared by mixing 5% or 10% PGM with 0, 50, 100, 150, or 300 mM BA, and the pH was adjusted to 8.0. The rheological properties of the mixtures were evaluated using a rheometer (Fig. 2). At 0 mM BA, for both 5% and 10% PGM-containing mixtures, G' was lower than G'', and the mixtures exhibited sol-like behavior. As the concentration of BA increased, G' gradually increased, indicating the formation of PGM/BA hydrogels. These results show that the gel strength of the PGM/BA hydrogels varies with the BA concentration. Interestingly, at 10 rad s^{-1}, the BA concentrations at which G' exceeded G'' varied depending on the PGM concentration (Fig. 2f). This transition occurred at approximately 100 mM for 5% PGM-containing mixtures, whereas it occurred at lower BA

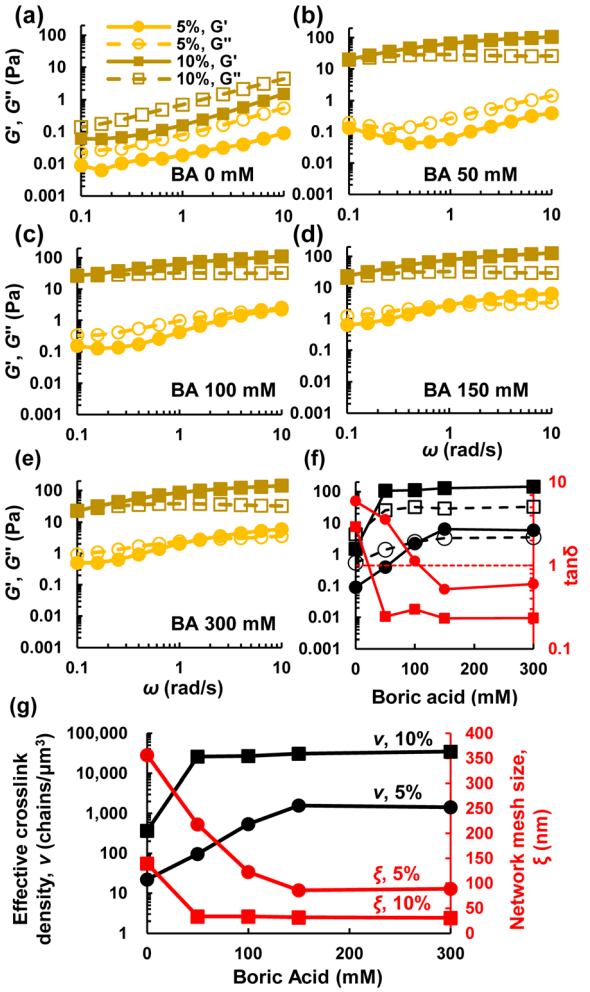

Fig. 2 Rheological properties of PGM/BA mixtures with varying BA concentrations. Mixtures containing 5% and 10% PGM were prepared with BA concentrations of (a) 0, (b) 50, (c) 100, (d) 150, and (e) 300 mM and adjusted to pH 8.0. Rheological measurements were conducted using a rheometer in frequency sweep mode at 10% strain. Filled and open symbols indicate the storage modulus (G′) and loss modulus (G″), respectively. (f) G' G'' and loss tangent (tanδ) values at 10 rad s^{-1} plotted as a function of the BA concentration. (g) Effective crosslink density (ν) and network mesh size (ξ) calculated from the G' value at 10 rad s^{-1}.

concentrations (estimated at 25 mM) for 10% PGM-containing mixtures. In addition, for both 5% and 10% PGM-containing mixtures, both G' and G'' plateaued after G' exceeded G''.

The effective crosslink density (ν) and network mesh size (ξ) were calculated from the G' value at 10 rad s^{-1} using the following equations (eqn (1) and (2)), where k_B is the Boltzmann constant and T is the measurement temperature (298 K).

$$\nu = \frac{G'}{k_B T} \quad (1)$$

$$\xi = \left(\frac{k_B T}{G'}\right)^{\frac{1}{3}} \quad (2)$$

As BA concentration increased, ν increased rapidly and plateaued at approximately 100–150 mM. Conversely, ξ decreased rapidly and then converged to a constant value (Fig. 2g). Because higher PGM concentration causes G' to exceed G'' at lower BA concentrations, the changes in ν and ξ can be attributed to increased mucin oligosaccharide density. The crosslinking between the BA and diol groups of the O-linked oligosaccharide proceeded efficiently, leading to the saturation of the crosslinking sites. The decrease in ξ with increasing ν is likely due to the spatial limitations imposed by the high molecular weight and branched structure of mucin. Particularly, at 10% PGM and low BA concentration (50 mM), high ν and small ξ values were observed, indicating a dense network structure with numerous crosslinking points.

This rapid network formation *via* multipoint crosslinking and subsequent saturation is a characteristic of physically crosslinked gels derived from branched polymers.[36,37] Higher PGM concentrations promote such network formation through multipoint crosslinking, forming high-density gels even at the same BA concentration. Hydrazide-crosslinked PVA hydrogels with linear chains exhibit ξ values of 15–50 nm.[38] Glutaraldehyde-crosslinked hydrogels exhibit ξ values ranging from 3 to 17 nm.[39] Fibrin gels exhibit ξ values of approximately 30–400 nm depending on gel concentration.[40] In the PGM/BA hydrogels developed in this study, ν values (10^4–10^5 chains μm^{-3}) and ξ values (50–500 nm) indicate a well-defined network structure characteristic of physically crosslinked multipoint gels.

The interconnected porous network structure of the PGM/BA hydrogel was also confirmed by SEM observations (Fig. S2), which support the mesh size estimated from rheological analysis.

Gel strength of PGM/BA hydrogel changes depending on PGM concentration

Building on the previous section, we evaluated the effect of PGM concentration on the rheological properties of the PGM/BA hydrogels. Mixtures containing 3%, 5%, or 10% PGM and 100 mM BA were prepared, and the pH of the mixtures was adjusted to 8.0. The rheological properties were measured using a rheometer (Fig. 3). The 3% PGM-containing mixture exhibited a sol-like behavior. As the PGM concentration increased, the mixture transitioned to a gel-like state. For the 10% PGM-containing mixture, the G' value at 10 rad s^{-1} reached approximately 100 Pa, and a hard hydrogel was formed that maintained its shape when lifted with tweezers (Fig. 3c). At 10 rad s^{-1}, G' exceeded G'' when the PGM concentration was >5%, indicating gel formation. These results demonstrate that the gel strength of the PGM/BA hydrogels increases with increasing PGM concentration. This behavior is likely due to the greater number of available crosslinking sites. More diol groups are available for crosslinking at higher PGM concentrations, facilitating network formation and enhancing gel strength.

PGM/BA hydrogel exhibits strong self-healing and adhesive properties

The self-healing properties of the PGM/BA hydrogels were evaluated. "Self-healing" refers to the ability of two cut gel

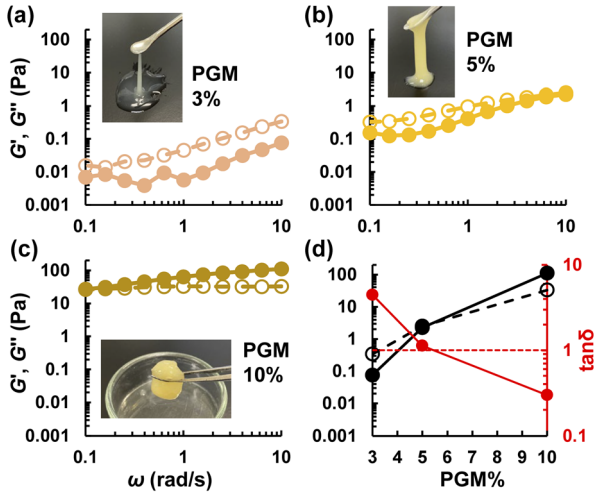

Fig. 3 Rheological properties of PGM/BA mixtures with varying PGM concentrations. The mixtures contained 100 mM BA and PGM concentrations of (a) 3%, (b) 5%, and (c) 10% and were adjusted to pH 8.0. Rheological measurements were performed using a rheometer in frequency sweep mode at 10% strain. Filled and open circles indicate the storage modulus (G') and loss modulus (G''), respectively. (d) G', G'' and loss tangent (tanδ) values at 10 rad s^{-1} plotted as a function of the PGM concentration.

pieces to rejoin into a single, continuous gel that does not separate when pulled from both sides.[41] Self-healing materials are considered promising for medical applications, such as wound healing, tissue bonding, and repair.[41,42] Given that mucin forms gel-like networks *via* molecular interactions[8–10] and that PVA/BA hydrogels exhibit self-healing properties,[43] we hypothesized that PGM/BA hydrogels would exhibit similar properties.

A PGM/BA hydrogel was prepared by mixing 10% PGM with 300 mM BA, and the pH was adjusted to 8.0. The hydrogel was stained with two dyes (Rhodamine 6G, red and methylene blue, blue) for visualization (Fig. 4a and Movie S1). The stained gels were cut in half using a spatula (Fig. 4a(I and ii)). The cut surfaces were brought into contact, gently pressed with a spatula, and allowed to rest for 1 min (Fig. 4a(ii–v)). These gels were manually pulled from both ends after 1 min (Fig. 4a(vi)). The gel remained intact as a single body, indicating self-healing. This property can be attributed to the rapid formation of physical crosslinks at the interface between the PGM and BA.

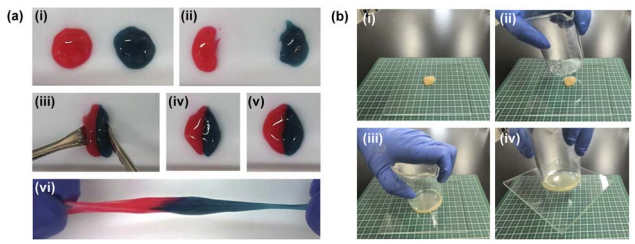

Fig. 4 Self-healing and adhesive properties of the PGM/BA hydrogel. Hydrogels were prepared by mixing 10% PGM with 300 mM BA, and the pH was adjusted to 8.0. (a) Self-healing behavior. (i) Hydrogels stained with two dyes (Rhodamine 6G and methylene blue). (ii) Stained hydrogels cut in half using a spatula. (iii) Cut surfaces brought into contact and gently pressed with a spatula. (iv) Appearance immediately after contact. (v) Appearance after 1 min of contact. (vi) Gels manually stretched after the healing process. These procedures were recorded in Movie S1. (b) Adhesive behavior (i–iii) hydrogel placed on a glass plate, brought into contact with the bottom of a glass beaker, and pressed manually from above for 10 s. (iv) Glass plate lifted by holding the glass beaker. These processes were recorded in movie S2.

We evaluated the self-healing performance in a semi-quantitative manner by varying the contact time between two cut gel pieces. Hydrogels rejoined after 60 s exhibited complete healing, whereas samples with 10 s contact time showed only partial healing, and those with 0 s showed no healing (Movies S1–S3). This clear time dependence demonstrates the progressive re-formation of reversible borate–diol crosslinks at the interface.

The adhesive properties of the PGM/BA hydrogels were also assessed (Fig. 4b and Movie S2). A hydrogel composed of 10% PGM and 300 mM BA (pH 8.0) was placed on a glass plate and pressed against the bottom of a glass beaker for approximately 10 s (Fig. 4b(i–iii)). Upon lifting the glass beaker, the glass plate adhered to it *via* the hydrogel and was lifted together (Fig. 4b(iv)). These results demonstrate that the PGM/BA hydrogel possesses strong adhesive properties.

In addition, the adhesion strength depended on the crosslinking ratio. Hydrogels prepared with 10% PGM showed markedly higher adhesion strength than those prepared with 5% PGM (Fig. S3). This difference is consistent with the denser and more interconnected network structures observed in SEM (Fig. S1) and the smaller mesh sizes estimated from rheological analysis (Fig. 2g). A higher PGM concentration increases the density of diol groups available for borate complexation, thereby increasing the number of effective intermolecular interactions at the gel–substrate interface, which likely contributes to enhanced adhesion. All hydrogels were prepared in the same aqueous medium; therefore, the observed variation arises from the crosslinking ratio rather than differences in the infusing liquid.

Beyond their mechanical and adhesive properties, the unique oligosaccharide-rich nature of mucin suggests that the PGM/BA hydrogels may be applicable to functional biomaterial systems. Mucin-derived surfaces have been reported to capture and inactivate bacteria,[44] and mucin-mimetic coatings can reduce biofouling on solid substrates.[45] These features indicate that the reversible mucin–borate hydrogel could serve as a basis for antibacterial capture, disinfection, and antifouling surface technologies.

Mechanical integrity of PGM/BA hydrogels after UV irradiation

Sterilization is crucial for cell culture and medical applications. Common sterilization methods include heating, autoclaving, electron beam irradiation, and UV irradiation.[46–48] Previous studies have shown that while mucin is relatively resistant to various sterilization methods, heat-based methods, such as autoclaving, can cause partial degradation or denaturation of

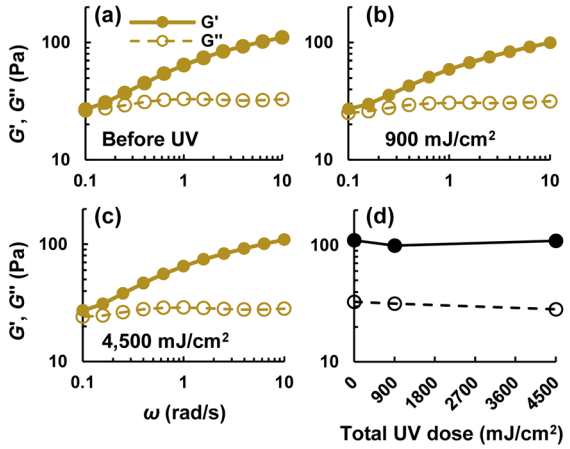

Fig. 5 Rheological properties of the PGM/BA hydrogels before and after UV irradiation. The hydrogels were prepared by mixing 10% PGM with 300 mM BA, and the pH was adjusted to 8.0. Rheological properties were evaluated (a) before UV irradiation, (b) after a total UV dose of 900 mJ cm^{-2}, and (c) after a total UV dose of 4500 mJ cm^{-2}. Measurements were performed using a rheometer in frequency sweep mode at 10% strain. Filled and open circles indicate the storage modulus (G') and loss modulus (G''), respectively. (d) G' and G'' values at 10 rad s^{-1} plotted as a function of UV dose.

mucin.[31] Given these limitations, we investigated the use of UV irradiation as a less thermally invasive sterilization method. To determine the suitability of UV irradiation for the sterilization of PGM/BA hydrogels, we examined whether UV exposure affected their mechanical properties. If the core proteins or oligosaccharides of PGM were denatured or degraded, a decrease in G' and G'' would be expected.

PGM/BA hydrogels were prepared by mixing 10% PGM with 300 mM BA, and the pH was adjusted to 8.0. Previous studies have shown that a total UV dose of approximately 10–200 mJ cm^{-2} from a low-pressure mercury lamp (LPML) is generally effective for >4-log microbial reduction.[49] However, because the luminous efficacy of an HPML at 254 nm is approximately five times lower than that of an LPML,[50] a dose of approximately 50–1000 mJ cm^{-2} is required when HPMLs are used.

To ensure sufficient exposure, we irradiated the samples using UV light at doses of 900 and 4500 mJ cm^{-2} using HPML. The rheological properties were evaluated before and after irradiation using a rheometer (Fig. 5). No significant changes in G' and G'' values at 10 rad s^{-1} were observed after UV irradiation (Fig. 5d), indicating that UV irradiation can sterilize PGM/BA hydrogels without compromising their mechanical integrity. Although mucin components may have been damaged locally, the overall network structure and gel strength were not compromised. Given the involvement of boric acid, cytocompatibility evaluation such as cell viability assays will be necessary for future biomedical applications.

Conclusions

In this study, we developed a reversible, physically crosslinked mucin-based hydrogel without chemical modification based on the pH-dependent interaction between the diol groups of mucin O-linked oligosaccharides and BA. Unlike previously reported mucin-based hydrogels formed by chemical crosslinking, this hydrogel was formed by the simple mixing of PGM and BA, followed by pH adjustment. It can be easily and reproducibly prepared without the irreversible alteration of the mucin structure.

The PGM/BA hydrogels exhibited reversible pH-dependent gelation behavior. By adjusting the concentrations of BA and PGM, the mechanical strength of the gel could be tuned, ranging from a soft gel to a robust, self-supporting structure. The increase in gel strength was associated with enhanced ν and reduced ξ; this behavior was attributed to dense multipoint crosslinking facilitated by the highly branched architecture of mucin molecules.

The gel also demonstrated a high self-healing ability, rejoining within 1 min of contact with cut surfaces and remaining intact when manually pulled. Furthermore, when placed between a glass plate and glass beaker, the PGM/BA hydrogel exhibited strong adhesive properties, effectively bonding the two surfaces. The mechanical strength of the hydrogel was retained after UV irradiation, indicating its resistance to UV-induced degradation and suitability for sterilization.

These features highlight the potential of the mucin-based hydrogel to preserve the physiological functions of mucin while providing self-healing ability, structural stability, and tunable mechanical properties. These features highlight the potential of the mucin-based hydrogel to preserve the physiological functions of mucin while providing self-healing ability, structural stability, and tunable mechanical properties. While the material shows promise, further cytocompatibility evaluation, including cell viability assays, will be essential before considering biomedical applications.

Author contributions

Yuki Nakamura: conceptualization, methodology, data curation, formal analysis, investigation, project administration, visualization, writing – original draft; Kanta Numata: resources, investigation; Momoka Hirosaki: methodology, investigation, visualization, Hiroki Miyajima: writing – review & editing; Satoshi Fujita: methodology, investigation, formal analysis, project administration, visualization, writing – review & editing.

Conflicts of interest

There are no conflicts to declare.

Data availability

The data supporting this article have been included as part of the main manuscript and the supplementary information (SI). Supplementary information is available. See DOI: https://doi.org/10.1039/d5na00731c.

Acknowledgements

This study was supported by the Recurrent Educational Support Program of the Kojima Fund of the Society of Fiber and Technology, Japan. We would like to thank Editage (https://www.editage.jp) for English language editing.

Notes and references

1 M. Andrianifahanana, N. Moniaux and S. K. Batra, *Biochim. Biophys. Acta, Rev. Cancer*, 2006, **1765**, 189–222.
2 P. Paone and P. D. Cani, *Gut*, 2020, **69**, 2232–2243.
3 R. Bansil and B. S. Turner, *Curr. Opin. Colloid Interface Sci.*, 2006, **11**, 164–170.
4 J. Dekker, J. W. A. Rossen, H. A. Büller and A. W. C. Einerhand, *Trends Biochem. Sci.*, 2002, **27**, 126–131.
5 M. Kesimer and J. K. Sheehan, *Methods Mol. Biol.*, 2012, **842**, 67–79.
6 G. Javitt, L. Khmelnitsky, L. Albert, L. S. Bigman, N. Elad, D. Morgenstern, T. Ilani, Y. Levy, R. Diskin and D. Fass, *Cell*, 2020, **183**, 717–729.e16.
7 G. Javitt, M. L. G. Calvo, L. Albert, N. Reznik, T. Ilani, R. Diskin and D. Fass, *J. Mol. Biol.*, 2019, **431**, 3740–3752.
8 M. Bäckström, D. Ambort, E. Thomsson, M. E. V. Johansson and G. C. Hansson, *Mol. Biotechnol.*, 2013, **54**, 250–256.
9 L. Arike and G. C. Hansson, *J. Mol. Biol.*, 2016, **428**, 3221–3229.
10 G. C. Hansson and M. E. V. Johansson, *Gut Microbes*, 2010, **1**, 51–54.
11 R. Bej and R. Haag, *J. Am. Chem. Soc.*, 2022, **144**, 20137–20152.
12 Y. H. Sheng and S. Z. Hasnain, *Front. Cell. Infect. Microbiol.*, 2022, **12**, 856962.
13 A. S. Luis and G. C. Hansson, *Cell Host Microbe*, 2023, **31**, 1087–1100.
14 J. F. Sicard, G. Le Bihan, P. Vogeleer, M. Jacques and J. Harel, *Front. Cell. Infect. Microbiol.*, 2017, **7**, 387.
15 C. Hou, W. He and X. Yao, *ACS Nano*, 2025, **19**, 14540–14556.
16 T. Deng, D. Gao, X. Song, Z. Zhou, L. Zhou, M. Tao, Z. Jiang, L. Yang, L. Luo, A. Zhou, L. Hu, H. Qin and M. Wu, *Nat. Commun.*, 2023, **14**, 396.
17 K. Jiang, H. Yan, C. Rickert, M. Marczynski, K. Sixtensson, F. Vilaplana, O. Lieleg and T. Crouzier, *Adv. Funct. Mater.*, 2021, **31**, 2008428.
18 M. Kretschmer, R. Ceña-Diez, C. Butnarasu, V. Silveira, I. Dobryden, S. Visentin, P. Berglund, A. Sönnerborg, O. Lieleg, T. Crouzier and H. Yan, *Adv. Sci.*, 2022, **9**, 2203898.
19 K. Joyner, D. Song, R. F. Hawkins, R. D. Silcott and G. A. Duncan, *Soft Matter*, 2019, **15**, 9632–9639.
20 G. D. Degen, C. A. Stevens, G. Cárcamo-Oyarce, J. Song, R. Bej, P. Tang, K. Ribbeck, R. Haag and G. H. McKinley, *Proc. Natl. Acad. Sci. U. S. A.*, 2025, **122**, e2415927122.
21 M. A. Momoh, M. U. Adikwu and S. O. Eraga, *Dhaka Univ. J. Pharm. Sci.*, 2008, **7**, 7–10.
22 A. W. Nugroho, H. Sosiati and P. Wijongko, *Int. J. Emerg. Trends Eng. Res.*, 2020, **8**, 2431–2437.
23 R. Nudelman, H. Alhmoud, B. Delalat, S. Fleicher, E. Fine, T. Guliakhmedova, R. Elnathan, A. Nyska, N. H. Voelcker, M. Gozin and S. Richter, *Adv. Funct. Mater.*, 2019, **29**, 1902783.
24 C. Tao, L. Peng, Q. Shao, K. Nan, R. Narain and Y. Chen, *Polym. Chem.*, 2025, **16**, 549–559.
25 R. Bej, C. A. Stevens, C. Nie, K. Ludwing, G. D. Degen, Y. Kerkhoff, M. Pigaleva, J. M. Adler, N. A. Bustos, T. M. Page, J. Trimpert, S. Block, B. B. Kaufer, K. Ribbeck and R. Haag, *Adv. Mater.*, 2024, **36**, e2401745.
26 C. Wang, Z. Shen, P. Hu, T. Wang, X. Zhang, L. Liang, J. Bai, L. Qiu, X. Lai, X. Yang and K. Zhang, *J. Sol-Gel Sci. Technol.*, 2022, **101**, 103–113.
27 R. Deleurence, T. Saison, F. Lequeux and C. Monteux, *ACS Omega*, 2018, **3**, 1864–1870.
28 B. Lu, F. Lin, X. Jiang, J. Cheng, Q. Lu, J. Song, C. Chen and B. Huang, *ACS Sustainable Chem. Eng.*, 2017, **5**, 948–956.
29 K. J. González-Morelo, M. Vega-Sagardía and D. Garrido, *Front. Microbiol.*, 2020, **11**, 591568.
30 Z. Li and W. Chai, *Curr. Opin. Struct. Biol.*, 2019, **56**, 187–197.
31 C. A. Rickert, T. M. Lutz, M. Marczynski and O. Lieleg, *Macromol. Biosci.*, 2020, **20**, 2000090.
32 D. Aminoff, W. D. Gathmann, C. M. Mclean and T. Yadomae, *Anal. Biochem.*, 1980, **101**, 44–53.
33 Q. Zhang, Z. Li and X. Song, *Front. Chem.*, 2020, **8**, 508.
34 Z. Guan, J. Lv, P. Bai and X. Guo, *Desalination*, 2016, **383**, 29–37.
35 Y. Zhang, Q. Chen and H. Watanabe, *J. Non-Newtonian Fluid Mech.*, 2023, **316**, 105012.
36 D. Yan, J. Chang, H. Zhang, J. Liu, H. Song, Z. Xue, F. Zhang and Y. Zhang, *Nat. Commun.*, 2020, **11**, 1180.
37 M. Rubinstein and A. N. Semenov, *Macromolecules*, 2001, **34**, 1058–1068.
38 N. R. Richbourg, M. Wancura, A. E. Gilchrist, S. Toubbeh, B. A. C. Harley, E. Cosgriff-Hernandez and N. A. Peppas, *Sci. Adv.*, 2021, **7**, eabe3245.
39 J. Karvinen, T. O. Ihalainen, M. T. Calejo, I. Jönkkäri and M. Kellomäki, *Mater. Sci. Eng., C*, 2019, **94**, 1056–1066.
40 A. R. Wufsus, K. Rana, A. Brown, J. R. Dorgan, M. W. Liberatore and K. B. Neeves, *Biophys. J.*, 2015, **108**(1), 173–183.
41 A. Devi V K, R. Shyam, A. Palaniappan, A. K. Jaiswal, T.-H. Oh and A. J. Nathanael, *Polymers*, 2021, **13**, 3782.
42 H. Omidian, R. L. Wilson and E. J. Gill, *Gels*, 2024, **10**, 241.
43 V. H. Luan and H. Long, *IOP Conf. Ser. Earth Environ. Sci.*, 2024, **1340**, 012004.
44 Z. Tan, X. Wang, Z. Wang, J. Jiang and X. Yao, *Adv. Sci.*, 2025, **12**, e03809.
45 S. Zheng, Y. Liu, J. Yao, R. Zhu, X. Yu and Z. Cao, *ACS Appl. Mater. Interfaces*, 2024, **16**(35), 46177–46190.
46 R. Shyam and A. Palaniappan, *Bioprinting*, 2023, **33**, e00294.
47 R. Galante, T. J. A. Pinto, R. Colaco and A. P. Serro, *J. Biomed. Mater. Res., Part B*, 2018, **106**, 2472–2492.
48 M. Tao, T. Ao, X. Mao, X. Yan, R. Javed, W. Hou, Y. Wang, C. Sun, S. Lin, T. Yu and Q. Ao, *Bioact. Mater.*, 2021, **6**, 2927–2945.
49 J. Kong, Y. Lu, Y. Ren, Z. Chen and M. Chen, *Water Cycle*, 2021, **2**, 23–31.
50 A. Tauchi, *J. sci. technol. lighting.*, 2020, **44**, 12–13.